

# Long-Circulating Drug-Dye-Based Micelles with Ultrahigh pH-Sensitivity for Deep Tumor Penetration and Superior Chemo-Photothermal Therapy

Cunfeng Song, Yugang Li, Tianliang Li, Yuming Yang, Zhicheng Huang, Jesús Martínez de la Fuente, Jian Ni, and Daxiang Cui\*

Nanocarriers for chemo-photothermal therapy suffer from insufficient retention at the tumor site and poor penetration into tumor parenchyma. A smart drug-dye-based micelle is designed by making the best of the structural features of small-molecule drugs. P-DOX is synthesized by conjugating doxorubicin (DOX) with poly(4-formylphenyl methacrylate-co-2-(diethylamino) ethyl methacrylate)-*b*-polyoligoethyleneglycol methacrylate (P(FPMA-co-DEA)-*b*-POEGMA) via imine linkage. Through the  $\pi$ - $\pi$  stacking interaction, IR780, a near-infrared fluorescence dye as well as a photothermal agent, is integrated into the micelles (IR780-PDMs) with the P-DOX. The IR780-PDMs show remarkably long blood circulation ( $t_{1/2\beta} = 22.6$  h). As a result, a progressive tumor accumulation and retention are presented, which is significant to the sequential drug release. Moreover, when entering into a moderate acidic tumor microenvironment, IR780-PDMs can dissociate into small-size conjugates and IR780, which obviously increases the penetration depth of drugs, and then improves the lethality to deep-seated tumor cells. Owing to the high delivery efficiency and superior chemo-photothermal therapeutic efficacy of IR780-PDMs, 97.6% tumor growth in the A549 tumor-bearing mice is suppressed with a low dose of intravenous injection (DOX, 1.5 mg kg<sup>-1</sup>; IR780, 0.8 mg kg<sup>-1</sup>). This work presents a brand-new strategy for long-acting intensive cancer therapy.

tumor site.<sup>[1]</sup> Even the drugs are loaded by nanocarriers, however, owing to the in vivo ubiquitous biological barriers (e.g., phagocytic sequestration, protein adsorption, and renal clearance),<sup>[2]</sup> only 0.7% of the injected dose can be effectively enriched in a solid tumor. Hence, the requirement to potent nanocarriers with high delivery efficiency becomes increasingly urgent.

Since the ability of being tailored from original polymers to achieve in vivo systemic administration, polymer micelles possess several unique properties, including toilless drug loading, controllable size tailoring, and adjustable function endowing, which makes them become one kind of ideal nanocarriers.<sup>[3]</sup> In order to obtain good therapeutic efficacy, blood circulation is one of the most important requirements.<sup>[4]</sup> Generally, long circulation of the micelles can promote the accumulation and retention of drugs at the tumor sites through the enhanced permeability and retention effect.<sup>[5]</sup> Recently, numerous studies have been devoted to the surface

modification of PEGylate and the size/charge adjustment of micelles to prolong the blood circulation time.<sup>[6]</sup> Nevertheless, these strategies can hardly cope with the fast clearance of drug caused by the early leakage to unexpected sites. Chemical cross-linking was used to stabilize polymeric micelles, but it does not necessarily promote the drug retention within the micelles.<sup>[7]</sup>

## 1. Introduction

The emerging nanocarriers tend to be more efficient and reliable for single-drug therapy of cancers. Nanocarriers can protect the bioactive components from degradation in physiological fluids, and provide a controlled release of drugs at the

Dr. C. Song, Dr. T. Li, Dr. Y. Yang, Z. Huang, Prof. J. M. de la Fuente, Prof. J. Ni, Prof. D. Cui  
Institute of Nano Biomedicine and Engineering  
Shanghai Engineering Research Center for Intelligent Instrument for Diagnosis and Therapy  
Department of Instrument Science & Engineering  
School of Electronic Information and Electrical Engineering  
Shanghai Jiao Tong University  
800 Dongchuan Road, Shanghai 200240, P. R. China  
E-mail: dx cui@situ.edu.cn

Dr. Y. Li  
State Key Laboratory of Metal Matrix Composites  
School of Materials Science and Engineering  
Shanghai Jiao Tong University  
800 Dongchuan Road, Shanghai 200240, P. R. China

Dr. Y. Yang, Prof. J. Ni, Prof. D. Cui  
National Center for Translational Medicine  
Collaborative Innovational Center for System Biology  
Shanghai Jiao Tong University  
800 Dongchuan Road, Shanghai 200240, P. R. China

Prof. J. M. de la Fuente  
Instituto de Ciencia de Materiales de Aragón (ICMA-CSIC)  
Universidad de Zaragoza  
50009 Zaragoza, Spain

 The ORCID identification number(s) for the author(s) of this article can be found under <https://doi.org/10.1002/adfm.201906309>.

© 2020 The Authors. Published by WILEY-VCH Verlag GmbH & Co. KGaA, Weinheim. This is an open access article under the terms of the Creative Commons Attribution-NonCommercial License, which permits use, distribution and reproduction in any medium, provided the original work is properly cited and is not used for commercial purposes.

DOI: 10.1002/adfm.201906309

As is well known, rapid tumor angiogenesis-induced heterogeneous vasculature will make a tumor microenvironment to be lack of nutrients (e.g., oxygen and glucose).<sup>[8]</sup> In order to adapt to the extremely harsh bioenvironment, most of the tumor cells usually evolve stronger viability. Therefore, the application of mono-chemotherapy is fairly limited due to the low therapeutic efficacy caused by drug resistance.<sup>[9]</sup> Photothermal therapy (PTT), which thermally ablates tumor cells by directly converting light radiation into heat energy with the PTT agents, is regarded as a preferable method for eliminating malignant cells.<sup>[10]</sup> The PTT agents strongly absorb near-infrared (NIR) light (650–900 nm) that can penetrate deep tissue without causing any damage.<sup>[11]</sup> Among them, IR780, a stable NIR heptamethine dye, has attracted tremendous attention for its outstanding photothermal conversion and remarkable properties in NIR fluorescence/photoacoustic (PA) imaging.<sup>[12]</sup> Furthermore, by combining with PTT, the efficacy of chemotherapy with a low dose can be obviously enhanced.<sup>[13]</sup> This is especially effective for DNA damaging chemodrugs (e.g., doxorubicin (DOX)), because the NIR-generated hyperthermia can interfere with DNA repair.<sup>[14]</sup> Since it integrates two therapeutic methods on a single platform, the chemo-phototherapy shows a “1+1>2” effect to inhibit tumor growth by the synergistic enhancement interaction.<sup>[15]</sup> Unfortunately, due to the tumor-associated fibroblasts, high interstitial fluid pressure, and dense extracellular matrix, most of the nanocarriers are restricted in perivascular

regions.<sup>[16]</sup> As a result, the locally inhomogeneous distribution of nanocarriers will trigger the incomplete killing of tumor cells, particularly at drug/heat-omitted areas. Even worse, the current dye-based nanocarriers lack a stimulus-responsive “switch” to overcome these hindrances in deep tumor delivery.<sup>[17]</sup>

In this work, a smart drug-dye-based micelle with ultrahigh pH-sensitivity was employed to improve the therapeutic efficacy of malignant tumor. IR780-PDMs ( $\approx 142$  nm) were prepared by the self-assembly of P-DOX and the loading of IR780. The non-covalent  $\pi$ - $\pi$  stacking interaction between conjugated DOX and IR780 increased the retention of the two small-molecule drugs in polymeric micelles. Comparing with the nonconjugated counterparts (IR780-Ms) constructed by the block polymer poly(2-(diethylamino) ethyl methacrylate)-*b*-poly(oligoethylene glycol methacrylate) (PDEA-*b*-POEGMA), IR780-PDMs showed obviously enhanced tumor accumulation and retention due to their long systemic circulation. As shown in **Figure 1**, there are two stages of the pH response in the delivery process. First, after arriving at the tumor sites (pH 6.5–7.0), IR780-PDMs dissociated into small-size conjugates and IR780. It has been found that the ultrasized particles ( $\approx 10$  nm) are inherently favorable to the deep penetration into tumor due to their low diffusional hindrance.<sup>[18]</sup> Second, once P-DOX is endocytosed into the intracellular endo/lysosome (pH 4.5–6.0), its aromatic imine linkage can be hydrolyzed,<sup>[19]</sup> which leads to a stimuli-triggered release of DOX. Such a combinatorial approach can

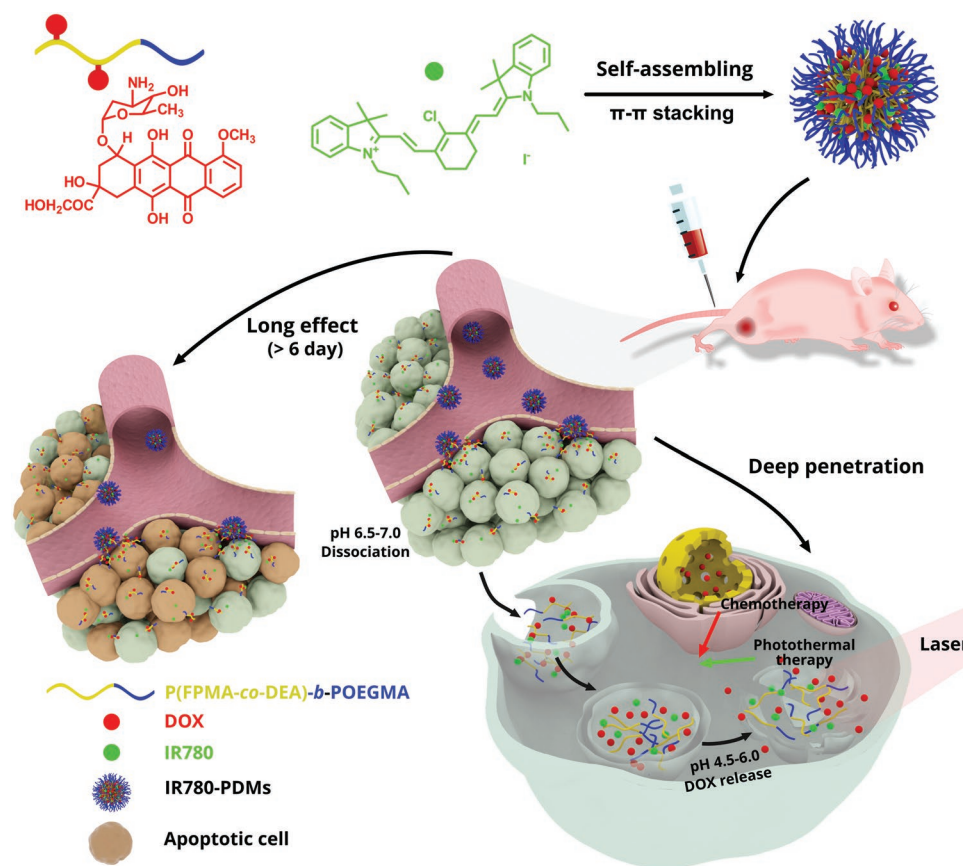


**Figure 1.** Schematic illustration of the self-assembly and  $\pi$ - $\pi$  stacking formation of IR780-PDMs with ultrahigh pH sensitivity, and their application in superior chemo-photothermal therapy.

overcome various physiological and pathological barriers to optimize the drug delivery efficiency for chemo-photothermal therapy. In addition, being different from traditional micelles which always need multiple dosage to maintain effective drug concentration at the tumor tissue,<sup>[20]</sup> the sustained drug release of our system after a single-dose injection can effectively reduce the dosing frequency and prevent the recurrence of malignant tumor owing to the long-term tumor retention. The therapeutic and biosafe benefits of IR780-PDMs are further demonstrated in the present study as well.

## 2. Results and Discussion

### 2.1. Synthesis and Characterization of P-DOX

The copolymer backbone of P-DOX was synthesized via reversible addition-fragmentation chain-transfer polymerization. The synthesis routes of P-DOX are shown in Figure S1A (Supporting Information). <sup>1</sup>H NMR spectra of all the polymers reveal that all the proton signals have a good correspondence with their molecular structures (Figure S1B, Supporting Information). After the Schiff base reaction between the amine group of DOX and the aldehyde group of poly(4-formylphenyl methacrylate-co-2-(diethylamino) ethyl methacrylate)-*b*-poly(oligoethyleneglycol methacrylate) (P(FPMA-co-DEA)-*b*-POEGMA), an increase of molecular weight can be observed, as shown in Figure S2 (Supporting Information). The number-average molecular weights ( $M_n$ ) and dispersity (PDI, polydispersity index) were analyzed by gel permeation chromatography (GPC; Table 1). Fourier transform-infrared spectroscopy (FT-IR) and UV-vis spectra were used to characterize P-DOX, which confirms the successful synthesis of this conjugate (Figures S3 and S4, Supporting Information).

The self-assembly of P-DOX into micellar structures in phosphate buffer (PB) solution (pH 7.4) was observed by transmission electron microscopy (TEM; Figure 2A). Moreover, the scattering intensities of P-DOX with the concentration ranging from 0.001 to 1 mg mL<sup>-1</sup> were recorded by NanoBrook Omni. As shown in Figure 2B, the inflection point corresponding to the critical micelle concentration (CMC) is 0.029 mg mL<sup>-1</sup>, which indicates that P-DOX was aggregated in the form of micelles (PDMs) even at very low concentration. To investigate the pH-triggered disassembly, PDMs were incubated in a series of PB solutions with pH values in the range from 7.4 to 6.3. A sharp size variation from 126.3 ± 5.6 nm at pH 7.4 to 12.1 ± 0.9 nm at pH 6.6 within a very narrow range of acidity was measured by dynamic light scattering (DLS; Figure 2C). When the pH of medium decreased to 6.6, PDMs dissociated into P-DOX conjugates (Figure 2D), due to the change of hydro-

philic-lipophilic balance induced by the protonated PDEA blocks. This conjecture was proven by the variation of zeta potential from  $-0.2 \pm 0.1$  to  $18.8 \pm 1.2$  mV (Figure 2E). In addition, zeta potential of  $23.1 \pm 0.6$  mV at pH 5.0 suggests that the P-DOX conjugates can be easily and well dispersed into endo/lysosome.

### 2.2. Stability, Photothermal Efficiency, and Responsive Chemodrug Release of IR780-PDMs

Using acetone as a co-solvent, IR780 dyes were dropped into P-DOX solution during the self-assembly process followed by the evaporation of acetone. The CMC value of P-DOX with IR780 is 0.022 mg mL<sup>-1</sup>, it is probably because the stacking interaction with the hydrophobic molecule makes the aggregation be easier to form the micelles (Figure S5A, Supporting Information). As shown in Figure 2F, after encapsulation, the hydrodynamic diameter of IR780-PDMs was  $142.8 \pm 3.7$  nm. The in vitro stability of IR780-PDMs was also investigated by DLS (Figure S5B, Supporting Information). The particle size of IR780-PDMs did not show significant variation after being incubated in both PBS and 10% fetal bovine serum (FBS) medium at pH 7.4 for 48 h. The pH of medium was instantaneously adjusted to 6.6 by adding 1 M HCl. Then, the time-dependent decrease of scattering intensity was measured, which reveals that the size transition of IR780-PDMs at acidic pH can be accomplished within 10 min (Figure S6, Supporting Information). Compared with our previous work,<sup>[21]</sup> this relative long dissociation time might be attributed to the strong  $\pi$ - $\pi$  stacking effect among the polymeric chains. Meanwhile, the dissociation of IR780-PDMs into small particles around 10 nm can be observed in Figure S7 (Supporting Information).

The photothermal behavior of IR780-PDMs was evaluated by monitoring the temperature variation under continuous laser irradiation (808 nm, 1 W cm<sup>-2</sup>). The visual images (Figure 2G) shows that there is a negligible change in the temperature of phosphate-buffered saline (PBS). However, a distinct change of the temperature of IR780-PDMs, which depends on the concentration of IR780, is observed. Figure 2H presents that the temperature of IR780-PDMs increased 17.5 °C at an equivalent concentration of 12 µg mL<sup>-1</sup> of IR780 within 5 min of irradiation. The heat converted from the laser can deal irreversible damage to cancer cells.

The drug loading percentages (DL) of DOX and IR780 were  $6.8 \pm 0.6\%$  and  $3.6 \pm 0.4\%$ , respectively. An effective anticancer agent should respond to a tumor-relative stimulus and then release drugs for therapy. In order to estimate the stimuli-sensitive drug releasing capacity, IR780-PDMs were dialyzed against PBS of different pH values. As shown in Figure 2, only 12.1% DOX was released from IR780-PDMs at pH 7.4 for 48 h, suggesting that most of DOX were embedded into micelles during blood circulation. By contrast, IR780-PDMs showed a much faster release at pH 5.0, up to 76.3%, which was even higher than the release at pH 6.6. The cumulative release of DOX from IR780-PDMs was remarkably accelerated in acidic environment, which can be attributed to the breaking of the acid-labile imine bonds. In addition, after the irradiation of 808 nm laser (1 W cm<sup>-2</sup>, 5 min), the release of DOX at pH 5.0 was further

**Table 1.** Characteristics of the polymers.

Sample	$M_n^a$	PDI <sup>a)</sup>
P(FPMA-co-DEA)	6920	1.27
P(FPMA-co-DEA)- <i>b</i> -POEGMA	34 579	1.34
P-DOX	38 168	1.40

<sup>a)</sup>Determined by GPC in DMF using PMMA as standards.

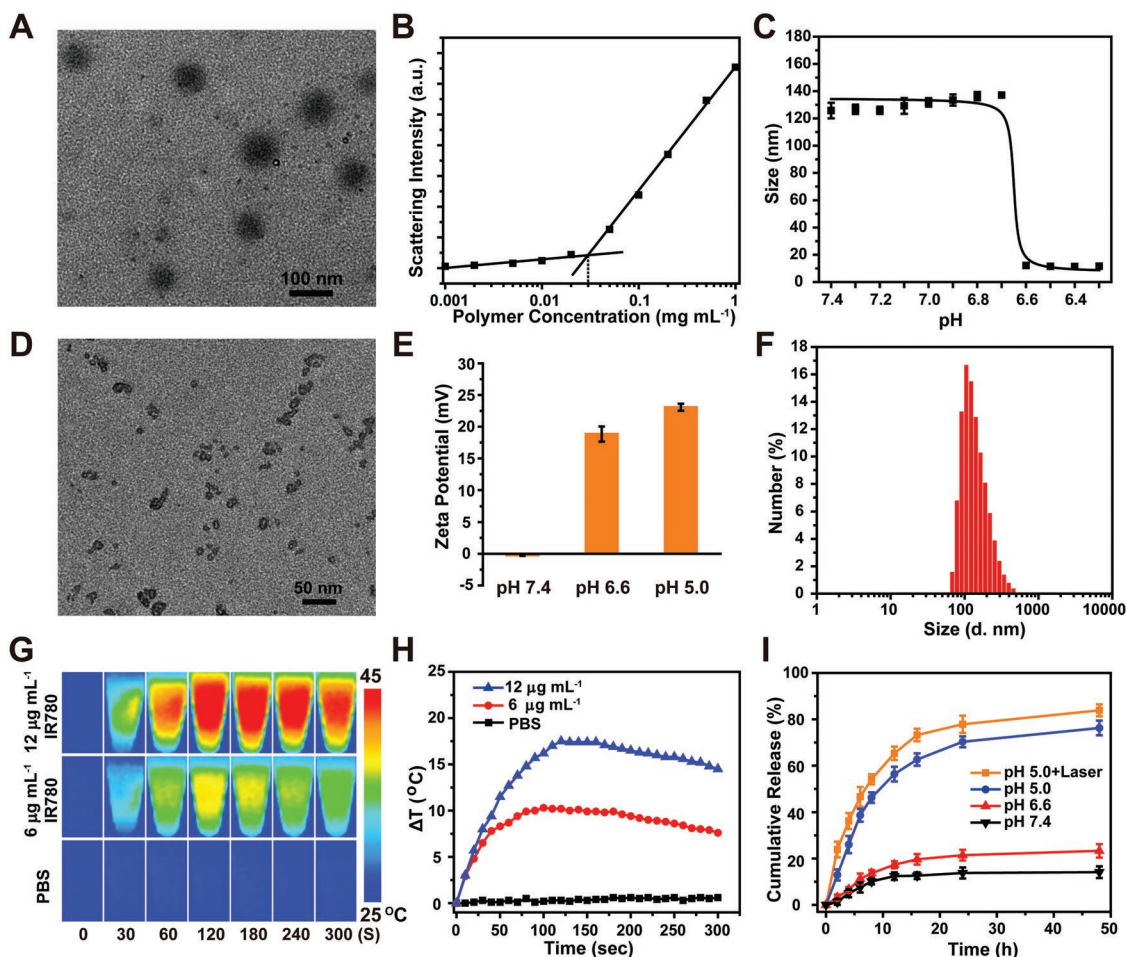


**Figure 2.** A) TEM image of PDMs, assembled by P-DOX at pH 7.4. B) Scattering intensity of P-DOX at different concentration. C) pH-dependent size change of PDMs. D) TEM image of P-DOX, dissociating from PDMs at pH 6.6. E) Zeta potential of PDMs at pH 7.4, 6.6, and 5.0. F) DLS of IR780-PDMs. G) Infrared thermal images and H) temperature changes of IR780-PDMs (equivalent to 6 or 12 mg mL<sup>-1</sup> IR780) in response to laser irradiation (808 nm, 1 W cm<sup>-2</sup>) within 300 s. I) In vitro release of DOX from IR780-PDMs at 37 °C.

increased to 83.9%, which is probably because the light-induced heat facilitated the hydrolysis of imine linkage and molecular diffusion. Therefore, the pH-dependent release property of IR780-PDMs is conducive to the intracellular targeting drug delivery. As shown in Figure S8 (Supporting Information), the cumulative release amount of the loaded IR780 was less than 15% at pH 7.4 within 48 h. However, the corresponding value at pH 6.6 increased up to 82.2%, which can be attributed to the dissociation of nanocarriers. Under laser irradiation, the release was most likely accelerated by the heat-triggered destruction of  $\pi$ - $\pi$  stacking interaction and the molecular diffusion.

### 2.3. Cytotoxicity and Cellular Uptake of IR780-PDMs

In vitro cytotoxicity was evaluated by 3-(4,5-dimethyl-2-thiazolyl)-2,5-diphenyl tetrazolium bromide (methyl thiazolyltetrazolium) (MTT) assay on A549 cell line. As shown in Figure 3A, due to the excellent biocompatibility of copolymer backbone P(FPMA-co-DEA)-*b*-POEGMA, no obvious cell death was observed in this group. Whereas, after the treatments with various drug

formulations for 24 h, the cell viability decreased with the increase of DOX concentration from 0.5 to 10  $\mu$ g mL<sup>-1</sup>. Free DOX, PDMs, and IR780-PDMs showed similar cytotoxicity to the tumor cells under the condition of pH 7.4. However, compared with the viabilities of cells that separately incubated with PDMs and IR780-PDMs at pH 6.6, the acidic environment gave rise to a lower survival rate, the reason of which might be the fact that more positive drug formulation had entered into cells. At both of the two pH values, the cell viabilities of IR780-PDMs with NIR laser were lower than those without NIR laser, and they decreased in pace with the increase of the concentration of IR780.

In order to further evaluate the photodamage effect of IR780-PDMs, A549 cells were stained by calcein AM/PI after the treatment in different conditions, and detected by fluorescence microscopy (Figure 3B). Live cells produce strong green fluorescence, while dead cells produce strong red fluorescence.<sup>[22]</sup> Whether with or without laser, there were almost all green spots in the control group. However, more red spots were observed in the IR780-PDMs group with laser radiation, which proved the obvious photothermal toxicity of IR780-PDMs to cells. The Annexin V-FITC/PI staining was employed to detect

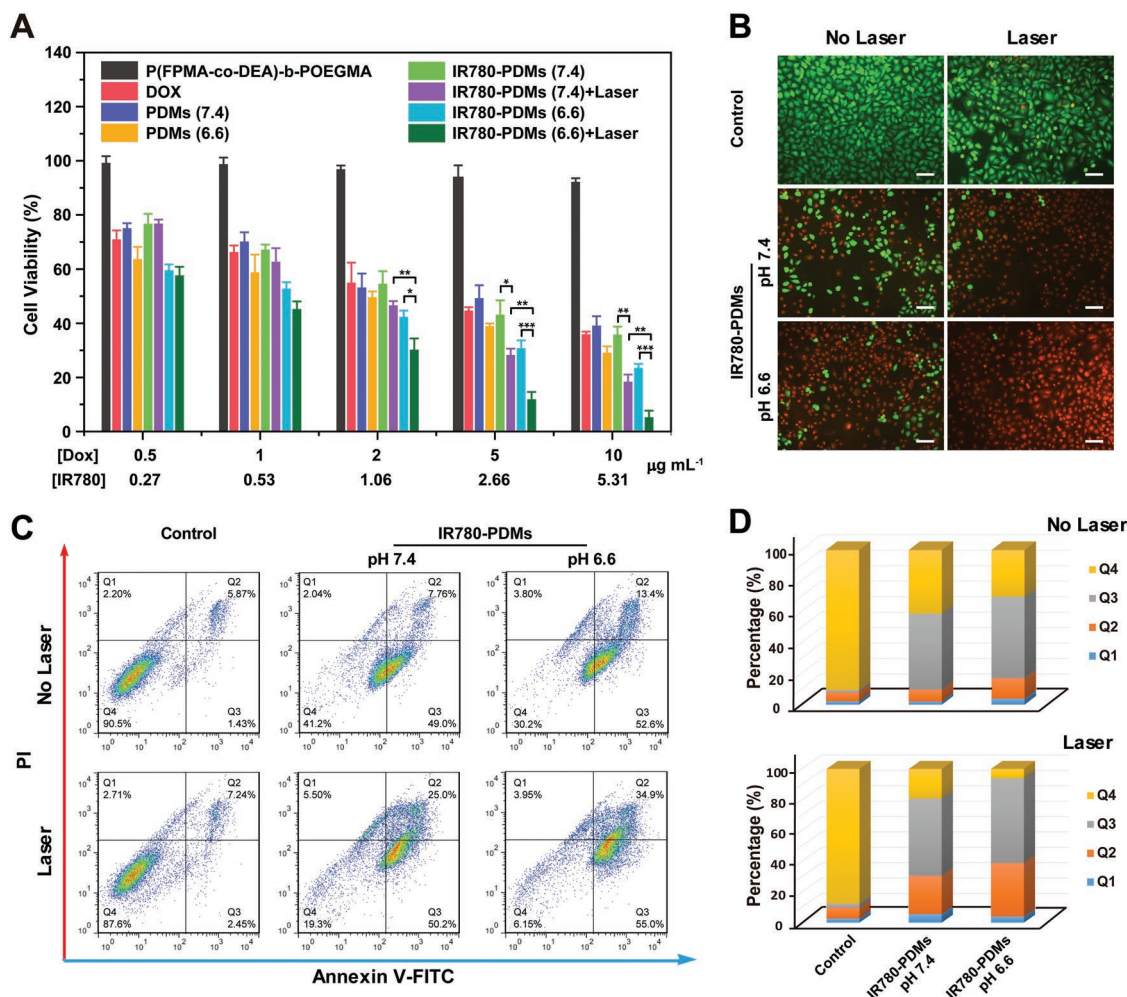


**Figure 3.** A) Viability of A549 cells incubated with different drug formulations with and without laser irradiation ( $1 \text{ W cm}^{-2}$ , 5 min).  $*p < 0.05$ ,  $**p < 0.01$ ,  $***p < 0.001$ . B) Fluorescence images and C) apoptosis assay of A549 cells treated with IR780-PDMs with and without laser irradiation ( $1 \text{ W cm}^{-2}$ , 5 min), PBS was used as a control. Q1: necrotic cells, Q2: later apoptotic cells, Q3: early apoptotic cells, Q4: living cells. Scale bar: 25  $\mu\text{m}$ . D) The relative changes of the percentage in each apoptosis quadrant.

the distribution of apoptotic cells (Figure 3C,D). Laser radiation induced significant cell apoptosis with apoptotic rates of 75.2% at pH 7.4 and 89.9% at pH 6.6, which were 1.3-fold and 1.4-fold higher than those of IR780-PDMs group without laser radiation at the corresponding pH conditions, respectively. Hence, it is clear that IR780-PDMs are capable of promoting tumor cell apoptosis by synergistic chemo-photothermal treatment.

The cellular uptakes of IR780-PDMs at pH 7.4 and 6.6 were evaluated by confocal laser scanning microscopy (CLSM) with the fluorescence intensities of DOX and IR780, respectively. As shown in Figure 4A, after incubation with IR780-PDMs at acidic pH for 1 h, the strong red fluorescence of DOX and green fluorescence of IR780 can be clearly observed in cells. Furthermore, these endocytosed carriers rapidly passed through lysosomes, and released DOX to nucleus. During the entire period of incubation time, the fluorescence signals of IR780-PDMs treatment at pH 6.6 were much stronger than those at pH 7.4. In addition, flow cytometry data further exhibited that the internalization of IR780-PDMs was much faster at pH 6.6 (Figure 4B,C). Considering the protonation of PDEA blocks

and the disassembly of IR780-PDMs in acidic environment, the possible reasons of these phenomena can be: 1) positive surface charge mediates more carriers entering into cells via the interaction with the negative cell membrane;<sup>[23]</sup> 2) size-dependent endocytosis accelerates the internalization of smaller ones.<sup>[24]</sup>

#### 2.4. Tumor Penetration of IR780-PDMs

Multicellular spheroids (MCSs), as 3D models which can accurately reflect the complex in vivo microenvironment, have been used in many research areas, including hepatotoxicity, neurology, and cancer biology.<sup>[25]</sup> The intratumoral penetration of IR780-PDMs was evaluated through co-incubation with A549 MCSs at different pH for 4 h. The maximal sections of MCSs were monitored by CLSM. After the treatment at pH 7.4, the red and green fluorescence mostly located at the marginal area of spheroid (Figure 5A). By contrast, these fluorescence signals distributed inside MCSs at pH 6.6, which indicated that the

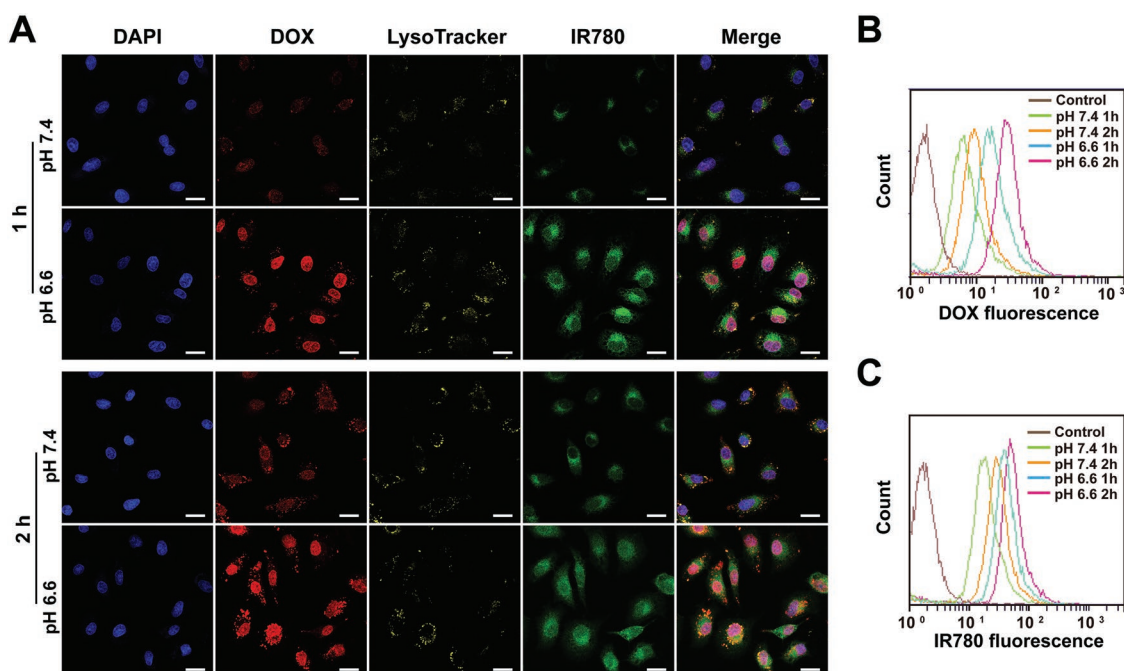


**Figure 4.** A) CLSM images and B,C) Flow cytometry analysis of A549 cells incubated with IR780-PDMs at pH 6.6 or 7.4 for 1 and 2 h. DAPI: blue signal, DOX: red signal, LysoTracker: yellow signal, IR780: green signal. Scale bar: 25  $\mu$ m.

penetration depth was also correlated with the dissociation of IR780-PDMs in acidic environment. Plots of the fluorescence intensity to the distance measured from the spheroid central axis reveal that the penetration depth of IR780-PDMs into MCSs at pH 6.6 was much deeper than that at pH 7.4 (Figure 5B).

To better demonstrate the penetration ability, the diffusion of IR780-PDMs into tumor was investigated by exposing them to excised cancer tissue in medium at pH 6.6 and pH 7.4, respectively. As shown in Figure 5C, IR780-PDMs exhibited minimal penetration ability at physiological pH, since the fluorescence was mostly located on the tumor edge. Whereas, more fluorescence signals of DOX and IR780 were observed from the inside of the excised tumor at acidic pH. The penetration ability can be enhanced by the dissociation of IR780-PDMs into small-size conjugates, which is consistent with the results of former researches.<sup>[18b,26]</sup> Further, the *in vivo* tumor penetration was investigated by the intravenous injection of IR780-PDMs into tumor-bearing nude mice (Figure 5D). Due to the pH-triggered dissociation of IR780-PDMs at the tumor tissue, the deep penetration can be clearly observed from the frozen sections of solid tumor which was collected at 24 h postinjection. After extravasation from the vessels, the fluorescence of DOX and IR780 was spreaded over the entire tumor parenchyma.

## 2.5. Tumor-Targeted Imaging of IR780-PDMs

A549 tumor-bearing BALB/c nude mice after intravenous injection with IR780+P-DOX and IR780-PDMs were captured by NIR-fluorescence/PA imaging system to evaluate the tumor-targeting efficiency *in vivo*. As depicted in Figure 6A, the fluorescence of IR780 in both groups almost distributed

all over the body of mice at 2 h postinjection. For the IR780-PDMs group, the fluorescence signal at the tumor site gradually increased and finally reached the maximum level at 24 h postinjection. Moreover, the strong signal was sustained in the subsequent period of testing time, which indicates that IR780-PDMs can effectively achieve tumor-specific targeting without a ligand. In contrast, the tumor fluorescence intensity in the mice treated with IR780+P-DOX was notably weak and decreased along with time after 24 h postinjection, the reason of which is their rapid clearance from the blood circulation. To further confirm the tumor-targeting ability and quantitatively estimate the biodistribution of drug-loading nanocarriers, tumors and the major organs (heart, liver, spleen, lung, and kidney) were collected at 36 h postinjection for *ex vivo* NIR- fluorescence imaging (Figure 6B). In contrast with other tissues, the IR780-PDMs group showed the highest fluorescence intensity at the tumor site, which was also 2.4 times stronger than that of the IR780+P-DOX group (Figure 6C).

PA is an emerging biomedical imaging technique based on the transition from absorbed photons to acoustic waves which are then detected and processed to form an image.<sup>[27]</sup> In our system, IR780, a superb PA contrast agent, was used to visualize the tumor morphology *in vivo*. As shown in Figure 6D, after intravenous injection of PBS, the tumor barely exhibited PA signal. On the contrary, the PA signals in the IR780+P-DOX and IR780-PDMs groups displayed a distinct increase at 24 h postinjection owing to the enrichment of IR780 in tumor tissues. More importantly, the PA signal of the IR780-PDMs group was 4.4-fold and 2.6-fold higher than that of the PBS and the IR780+P-DOX groups (Figure 6E), respectively. Such a strong signal was all over the whole tumor, which can be attributed to the great tumor accumulation and permeation of IR780-PDMs.

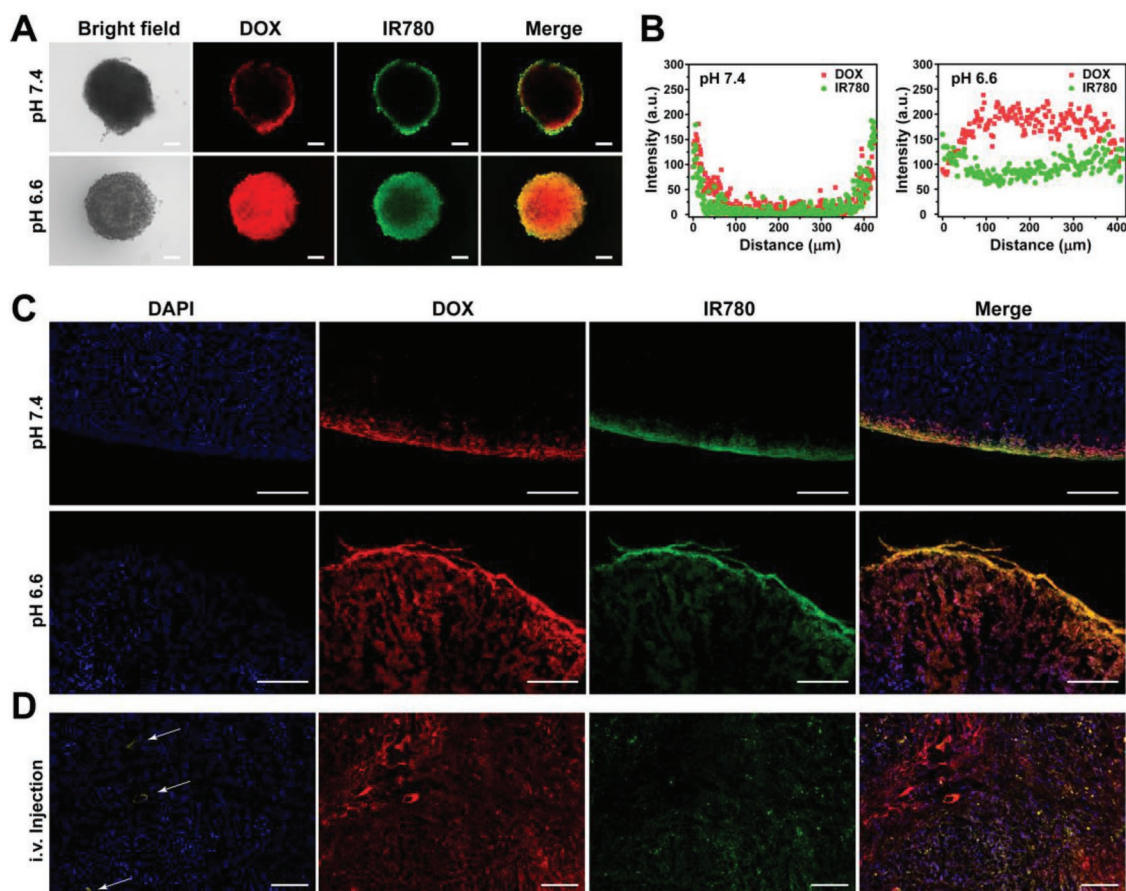


**Figure 5.** A) CLSM images of A549 MCSs for the ex vivo penetration test. The MCSs were incubated with IR780-PDMs for 4 h at pH 6.6 or 7.4. Scale bar: 100  $\mu\text{m}$ . B) Plots of the penetration depth of DOX and IR780 into A549 MCSs treated with IR780-PDMs. C) Frozen sections of A549 tumors after ex vivo incubation with IR780-PDMs solution for 4 h at pH 6.6 or 7.4. Scale bar: 200  $\mu\text{m}$ . D) Frozen section of A549 tumors after the intravenous administration of IR780-PDMs at 24 h postinjection. Arrows: CD31 antibody-labeled vascular endothelial cells. Scale bar: 100  $\mu\text{m}$ .

## 2.6. Circulation Half-Life and Tumor Retention of IR780-PDMs

To investigate the effect of the  $\pi$ - $\pi$  stacking of DOX and IR780 on the circulation half-life of polymeric micelles, the non-conjugated counterparts (IR780-Ms) self-assembled by block polymer (PDEA-*b*-POtEGMA) were used as the control group. The synthetic route of PDEA-*b*-POEGMA and the preparation process of IR780-Ms are presented in Figure S9 (Supporting Information). The interaction between IR780 and nanoparticles were analyzed by UV-vis spectra (Figure S10, Supporting Information). After loading IR780, a strong characteristic adsorption peak of IR780-PDMs appeared at 799 nm, with a red shift from 792 nm (free of IR780 and IR780-Ms), which was caused by the formation of  $\pi$ - $\pi$  stacking interaction.<sup>[28]</sup> Meanwhile, the red shift also appeared in the adsorption peak of DOX. In addition, the CMC and in vitro stability of IR780-Ms were investigated as well. As shown in Figure S11 (Supporting Information), the formation of the micelles requires a relatively high concentration (0.047 mg mL<sup>-1</sup>) of PDEA-*b*-POEGMA. Moreover, a drastic particle size variation of IR780-Ms in 10% FBS medium was observed within 48 h. Compared with IR780-PDMs, the nonconjugated micelles are unstable in complex surrounding.

The fluorescence of collected blood and the relative plasma levels of IR780 at different time points after the intravenous injections of free IR780, IR780-Ms, and IR780-PDMs are illustrated in Figure 7A,B. The fluorescence signals of free IR780 and IR780-Ms were rapidly eliminated from the systemic circulation, indicating that IR780 was very likely leaked from IR780-Ms and consequently metabolized from kidney. As being expected, IR780-PDMs displayed an evidently long elimination half-life ( $t_{1/2\beta} = 22.6$  h), which was about 11.9-fold and 8.4-fold longer than that of IR780 and IR780-Ms, respectively. These results implied the superior stability of IR780-PDMs which prevented the early drug leakage, and prolonged the blood circulation time.

The tumor accumulation and retention of free IR780, IR780-Ms, and IR780-PDMs were further evaluated by an IVIS Spectrum Imaging System (Figure 7C). IR780-PDMs exhibited great passive targeting ability and persisted to permeate into the tumor tissue over several days, which are beneficial to maintain effective drug concentration, and then reduce the dosing frequency. However, both free IR780 and IR780-Ms showed less tumoral uptake and shorter local retention time. Figure 7D reveals that the fluorescence intensity of excised tumor of the IR780-PDMs group at 6 days postinjection was nearly 9.7-fold

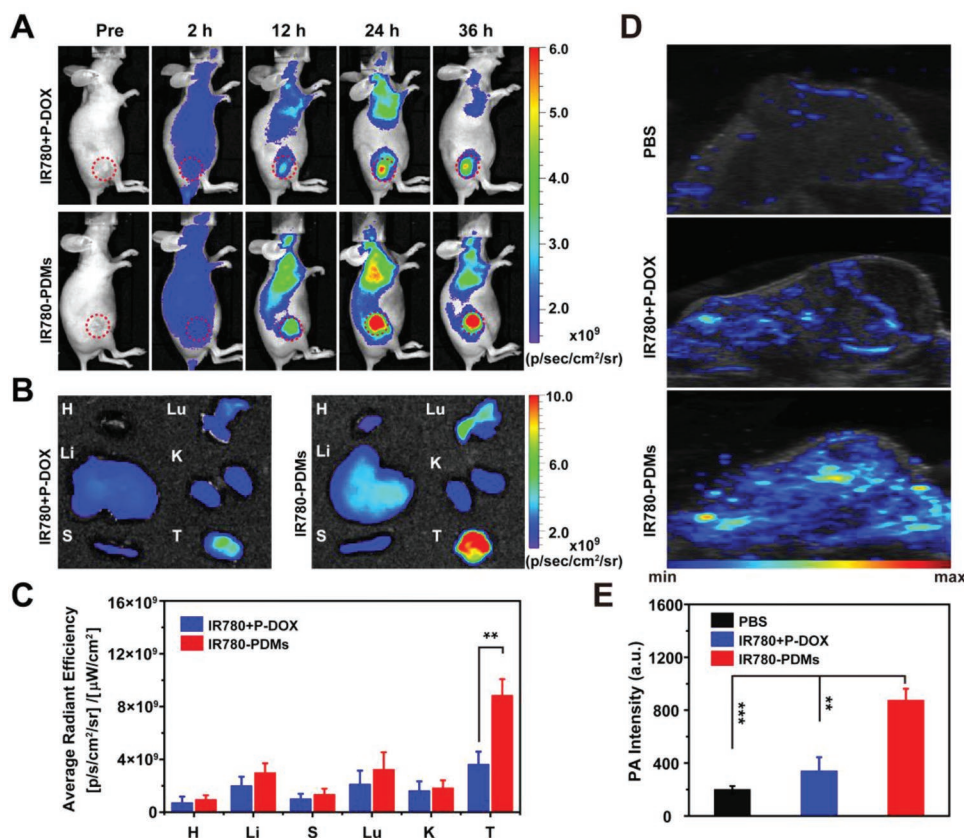


**Figure 6.** A) NIR fluorescence imaging of A549 tumor-bearing BALB/c nude mice taken at 2, 12, 24, and 36 h after intravenously administrated with IR780+P-DOX or IR780-PDMs. B) Ex vivo NIR fluorescence imaging and C) Quantitative analysis of the harvested organs and tumors at 36 h postinjection. D) PA imaging and E) PA intensity of tumor site after the intravenous administration of IR780+P-DOX or IR780-PDMs at 24 h postinjection. PBS as the control group. \*\* $p < 0.01$ , \*\*\* $p < 0.001$ .

and 6.5-fold higher than that of the free IR780 and IR780-Ms groups, respectively. Hence, through the  $\pi$ - $\pi$  stacking interaction, the small-molecule drugs were locked into the polymeric micelles, which obviously prolonged the blood circulation and further enhanced the tumor accumulation and retention of IR780-PDMs.

## 2.7. Chemo-Photothermal Synergistic Therapy and Biosafety of IR780-PDMs

Encouraged by the high photodamage and excellent tumor-targeting of IR780-PDMs, the in vivo photothermal experiments on A549 tumor-bearing mice were carried out at 24 h postinjection after treatment with PBS, IR780+P-DOX, or IR789-PDMs (Figure 8A). After 2 min of laser irradiation, the tumor of mice treated with IR789-PDMs reached a temperature over 45 °C. When the tumor site was exposed to 808 nm NIR laser for 5 min, the temperature for the IR789-PDMs group reached the maximum of 48.9 °C, with an increment of 16.9 °C. It has been demonstrated that the cancer cells, which are particularly vulnerable to heating, can be selectively killed by the nanocarrier-mediated hyperthermia with minimal damage to the surrounding normal cells.<sup>[29]</sup> However, the tumor temperature only reached 40.1 °C for the IR780+P-DOX group and 36.0 °C for

the PBS group ( $\Delta T < 8$  °C), which are far insufficient to induce cell necrosis. The tumor temperature decreased after turning off the irradiation (Figure S12, Supporting Information).

As shown in Figure 8B, a clear injury can be observed at the tumor site of mice treated with IR780-PDMs under laser irradiation. All of the tumors disappeared without recurrence accompanying with the shedding of solid scar and the regeneration of normal tissue. As for the another two-treated groups, there was no significant photothermal damage to the tumor tissue. The chemo-photothermal antitumor efficacy of IR780-PDMs was further investigated on A549 tumor-bearing mice. Figure 8C shows the tumor growth curves of mice treated with PBS, DOX, IR780+P-DOX, and IR780-PDMs, respectively. In the PBS-treated group, the tumor volumes grew rapidly and reached 1026 mm<sup>3</sup> at 18 days after the treatment, which can hardly be inhibited by the NIR laser irradiation. The groups treated by DOX and IR780+P-DOX with or without NIR laser irradiation showed negligible inhibition on tumor growth, which is because of the lower accumulation of DOX and IR780 at the tumor site. By contrast, 45.7% tumor suppression was obtained in the group treated with IR780-PDMs. Being combined with NIR laser irradiation, the tumor growth was noticeably inhibited, which showed a suppression ratio as high as 97.6% after the entire treatment cycle. The above results were further confirmed by the tumors weight at the end of the

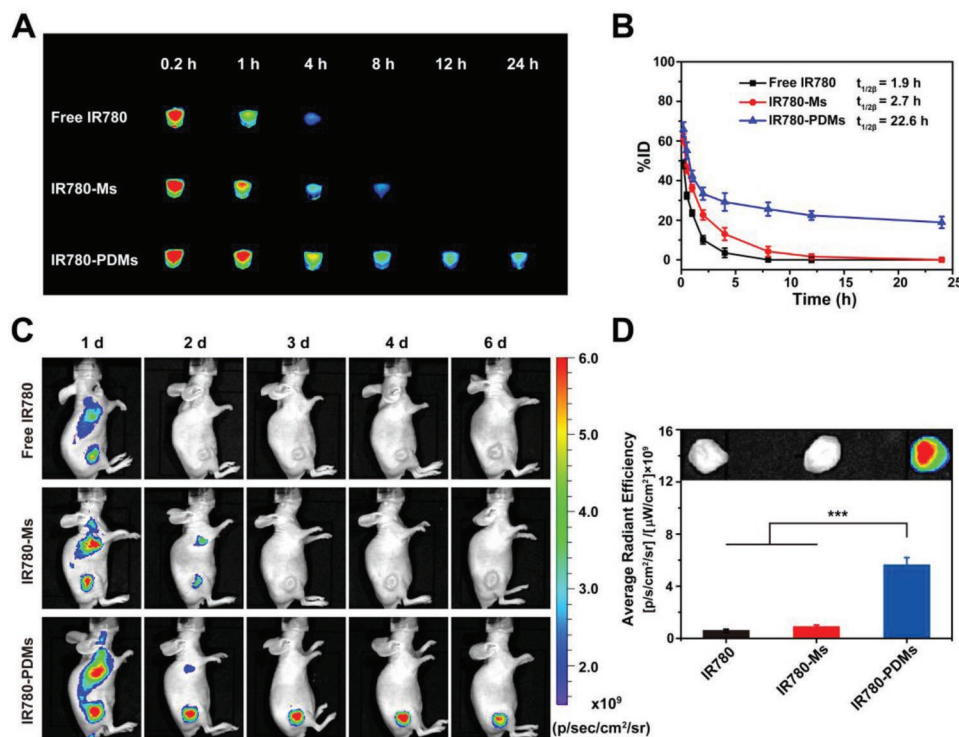


**Figure 7.** A) Fluorescence images of collected blood from mice at predesigned time after intravenous injection of free IR780, IR780-Ms, or IR780-PDMs. B) Circulation kinetics of different drug formulations. C) NIR fluorescence imaging of A549 tumor-bearing BALB/c nude mice at different time posts after intravenous injection of free IR780, IR780-Ms, or IR780-PDMs. D) Fluorescence intensities of the harvested tumors at 6 days postinjection.

therapies (Figure S13, Supporting Information). Hematoxylin and eosin (H&E) and TUNEL (terminal deoxynucleotidyl transferase-mediated dUTP nick end labeling) staining were used to estimate the cell apoptosis in tumor tissues (Figure 8D). Different from the typically histologic characteristics of malignant tumors such as hyperchromatic nuclei and scant cytoplasm,<sup>[30]</sup> obvious nuclear shrinkage and fragmentation were observed in the tumor slices of the group treated by IR780-PDMs with laser irradiation. Compared with the traditional drug-loaded nanocarriers for sole or synergistic tumor therapy,<sup>[12a,31]</sup> IR780-PDMs for chemo-photothermal therapy presented a superior tumor elimination effect at low dose as a result of the long-acting intensive therapeutic strategy.

The potential biosafety of IR780-PDMs was also evaluated. As shown in Figure 8E, the body weights of the mice slightly increased within an 18 days therapy. Moreover, the major organs of the mice at the end of the treatment, including heart, liver, spleen, lung, and kidney, were further analyzed by histological examination. The chemo-photothermal effects of IR780-PDMs caused no apparent pathological abnormalities or lesions (Figure S14, Supporting Information). These data suggested that IR780-PDMs have good biocompatibility to living animals and tremendous potential to be used as a promising antitumor agent.

### 3. Conclusion

In summary, we have successfully developed a smart drug-dye-based micelle to optimize tumoral delivery efficiency and reduce

systemic side effect of the drugs. Through the self-assembly of polymeric conjugates and  $\pi$ - $\pi$  stacking of small-molecule drugs, IR780-PDMs were constructed for chemo-photothermal therapy. Long-circulation of IR780-PDMs led to the enhancement of tumor accumulation and retention (up to 6 days), and consequently the extension of effect time against tumor cells. Furthermore, the enhanced penetration and controllable drug release of IR780-PDMs, due to their size conversion and bond fracture in response to tumor acidic microenvironment, were confirmed by both in vitro and in vivo experiments. IR780-PDMs showed high delivery efficiency, excellent synergistic antitumor effect, and fairly good biosafety after a single-dose intravenous injection into mice. Overall, this work presents a brand-new strategy for long-acting intensive cancer therapy which can overcome multiple biological obstacles.

### 4. Experimental Section

**Materials:** PFMA was synthesized according to the previous report.<sup>[32]</sup> The synthetic raw materials, 4-cyano-4-(phenylcarbonothioylthio) pentanoic acid (CPAD), azodiisobutyronitrile (AIBN), OEGMA, DEA, and doxorubicin hydrochloride (DOX-HCl) were purchased from J&K (China). FBS, trypsin, and Ham's F-12K medium were purchased from Gibco (USA). MTT, 4',6-diamidino-2-phenylindole (DAPI), and Annexin V-FITC/PI apoptosis detection kit were obtained from Beyotime (China). LysoTracker Green DND-189 were purchased from Yesen (China). All reagents in analytical grade were used as received. The dialysis membranes (MWCO: 3500 Da) were obtained from Sangon Biotech (China). Milli-Q water was purified via the Milli-Q Plus System (Millipore, USA).

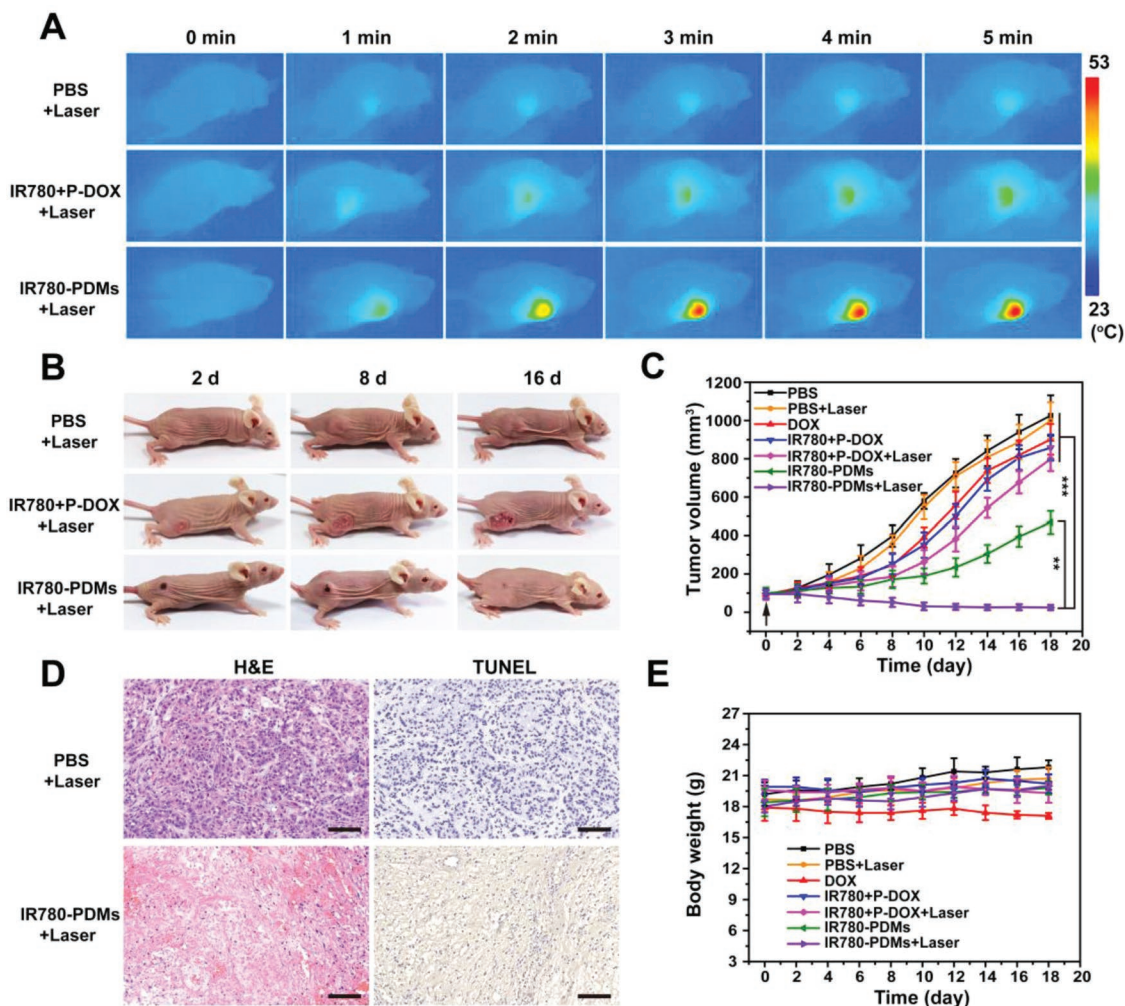


**Figure 8.** In vivo chemo-photothermal therapy. A) Infrared thermal images and B) representative images of mice treated with PBS, IR780+P-DOX, or IR780-PDMs. At 24 h postinjection, the mice were irradiated by 808 nm laser with the power of  $1 \text{ W cm}^{-2}$ . C) Tumor growth curves and E) body weight variation of A549 tumor-bearing mice treated with PBS, DOX, IR780+P-DOX, or IR780-PDMs. Laser: 808 nm,  $1 \text{ W cm}^{-2}$ , 5 min. (dose:  $1.5 \text{ mg kg}^{-1}$  DOX and  $0.8 \text{ mg kg}^{-1}$  IR780).  $^{**}p < 0.01$ ,  $^{***}p < 0.001$ . D) H&E and TUNEL staining images of tumor slices after different treatment. Scale bar:  $100 \mu\text{m}$ .

**Cells and Animals:** Human non-small-cell lung cancer cells (A549), provided by Chinese Academy of Sciences, were grown in Ham's F-12K supplemented with 10% FBS at  $37^\circ\text{C}$  under 5%  $\text{CO}_2$  in ESCO cell incubator. Female BALB/c-nude mice (5 weeks old) and BALB/c mice (6 weeks old) were ordered from Shanghai JSJ Laboratory Animal Co., Ltd. (China). All animal experiments were performed in compliance with the Guidelines for Use and Care of Animals in Shanghai Jiao Tong University.

**Synthesis of Copolymer Backbone:** P(FPMA-co-DEA)-b-POEGMA was synthesized in two steps. First, CPAD (35 mg, 0.125 mmol), AIBN (8.2 mg, 0.5 mmol), DEA (2.775 g, 15 mmol), and FPMA (0.950 g, 5 mmol) were dissolved in dry tetrahydrofuran (THF; 6 mL). The solution mixtures were subjected to five freeze-pump-thaw cycles and filled with argon in Schlenk tube. This sealed tube was immersed in a preheated oil bath at  $65^\circ\text{C}$  for 12 h. The resultant mixture was dialyzed against dimethylformamide (DMF) to remove unreactive monomers. Then, the obtained P(FPMA-co-DEA) (0.5 g, 0.05 mmol), AIBN (4.1 mg, 0.25 mmol), and OEGMA (1.5 g, 3 mmol) were dissolved in 4 mL of dry THF and degassed by performing five freeze-pump-thaw cycles. The reaction mixture was transferred into a preheated oil bath at  $65^\circ\text{C}$  for 12 h. P(FPMA-co-DEA)-b-POEGMA was purified by dialysis as described above.

**Fabrication of P-DOX:** P(FPMA-co-DEA)-b-POEGMA (0.4 g) was dissolved in 2 mL of DCM. DOX-HCl (50 mg) and threefold molar

triethylamine were dissolved in 2 mL of dimethyl sulfoxide for 2 h, and then dropwise added to the copolymer solution under stirring for an extra 16 h. The conjugates were isolated from the mixture by successive dialysis against sufficient DMF/deionized water and obtained by freeze-drying.

**Preparation of IR780-PDMs:** 5 mg of P-DOX was dissolved in 0.5 mL of acetone, and slowly injected into 5 mL of deionized water. 0.25 mg of IR780 with the concentration of  $1 \text{ mg mL}^{-1}$  in acetone was added to the conjugates. The final solution was kept stirring to evaporate the acetone completely, and then filtered through a  $0.45 \mu\text{m}$  Millipore filter.

**Characterization:** GPC (Waters ACQUITY UPLC, USA) was used to detect the molecular weight of copolymers, using polymethyl methacrylate (PMMA) standard with a refractive index detector and DMF as the elution. The chemical structures of copolymers were recorded on  $^1\text{H}$  NMR (Bruker, Germany), FT-IR (Thermo Nicolet, USA), and UV-vis absorption spectra (Shimadzu, Japan). DLS and zeta potential were performed by a Malvern Nanozetasizer (England). The scattering intensity of copolymer was monitored by NanoBrook Omni (USA). The morphologies were determined by TEM (JEOL, Japan) at 120 KV.

$150 \mu\text{L}$  of IR780-PDMs solutions (IR780-equivalent dose: 6 and  $12 \mu\text{g mL}^{-1}$ ) were placed in centrifuge tubes and exposed to NIR irradiation (808 nm continuous-wave diode laser,  $1 \text{ W cm}^{-2}$ ) for

5 min. PBS was also irradiated as a control. The temperature changes at different irradiation times were monitored by an IR thermal camera and analyzed using IR Flash thermal imaging software.

The fluorescence of DOX at excitation wavelength of 480 nm and IR780 at excitation wavelength of 720 nm were detected by F-4600 spectrofluorometer (Hitachi, Japan). The DL was calculated by the following formula: DL (%) = (weight of loaded drug) / (total weight of micelles and drug) × 100%.

**In Vitro Chemodrug Release Profile:** The DOX and IR780 release from IR780-PDMs was studied by the dialysis method. 1 mL of IR780-PDMs solution was placed into a dialysis membrane with or without laser irradiation (1 W cm<sup>-2</sup>, 5 min), and then incubated in 20 mL of PBS (pH 5.0, 6.6, or 7.4). The release experiments were carried out in an incubator under gentle sharking (100 rpm) at 37 °C. 0.5 mL of supernatant was taken at predetermined time intervals for detection, and then replaced by an equal volume of fresh release medium. The cumulative quantities of the DOX and IR780 released from IR780-PDMs were calculated based on the fluorescence emission intensity.

**Cytotoxicity and Apoptotic Assay:** A549 cells were seeded in 96-well plates at a density of 1 × 10<sup>4</sup> cells per well overnight. 150 µL of fresh medium containing P(DEA-co-FPMA)-*b*-POEGMA, DOX, PDMs, or IR780-PDMs (DOX-equivalent dose: 0.5–10 µg mL<sup>-1</sup>, IR780-equivalent dose: 0.27–5.32 µg mL<sup>-1</sup>) was separately added for incubation at pH 6.6 or 7.4 for 12 h. All the cells were washed twice with PBS, and treated with or without laser irradiation (1 W cm<sup>-2</sup>, 5 min). After another 12 h of incubation, the cellular cytotoxicity was determined by MTT assay. The absorbance of purple formazan crystals produced by live cells was recorded on Microplate Reader (Model 680, Bio-Rad). The relative cell viability was determined by comparing with the untreated cells.

Apoptosis induced by IR780-PDMs was detected using Annexin V-FITC/PI apoptosis detection kit. A549 cells were seeded in 24-well plates at 6 × 10<sup>4</sup> cells per well overnight before the exposure to IR780-PDMs (DOX-equivalent dose: 5 µg mL<sup>-1</sup>, IR780-equivalent dose: 2.66 µg mL<sup>-1</sup>) at pH 6.6 and 7.4 for 12 h, respectively. All the cells were washed with sufficient PBS, and irradiated with or without a power of 1 W cm<sup>-2</sup> 808 nm laser for 5 min. The following procedures were performed in accordance with the manufactures' protocols after an extra 12 h of incubation. The apoptotic and necrotic cell distributions were analyzed by Flowjo software.

The photodamage of cells caused by the carriers was visually observed by fluorescence microscopy. A549 cells were incubated with IR780-PDMs (DOX-equivalent dose: 5 µg mL<sup>-1</sup>, IR780-equivalent dose: 2.66 µg mL<sup>-1</sup>) at pH 6.6 or 7.4 for 12 h, and then washed with PBS twice. After being treated by the same laser exposure process as previous and incubation, the cells were stained with a mixture of Calcein-AM (2.0 × 10<sup>-6</sup> M)/PI (1.5 × 10<sup>-6</sup> M) and then observed by a Lecia CTR6000 fluorescence microscopy.

**Cellular Uptake:** A549 cells were seeded in a 24-well plate covered with glass at a density of 6 × 10<sup>4</sup> cells per well overnight. Subsequently, the cells were treated with IR780-PDMs (DOX-equivalent dose: 5 µg mL<sup>-1</sup>, IR780-equivalent dose: 2.66 µg mL<sup>-1</sup>) at pH 6.6 and 7.4 for 1 and 2 h, respectively. Afterward, the cells were washed twice with PBS, and then stained with LysoTracker to label lysosome. The nuclei of the cells were stained with DAPI, and then observed by a TCS SP8 STED confocal fluorescence microscopy (Leica, German). The intracellular uptake of IR780-PDMs was analyzed by flow cytometry.

**Penetration Assay:** A549 cells were 3D cultured by using the Corning spheroid microplate in accordance with the guidelines of forming MCSs. The medium was separately adjusted to pH 6.6 and 7.4, followed by the addition of IR780-PDMs (DOX-equivalent dose: 5 µg mL<sup>-1</sup>, IR780-equivalent dose: 2.66 µg mL<sup>-1</sup>). After 4 h incubation, MCSs were thoroughly washed with PBS and monitored by Leica TCS SP8 CLSM Z-stack scanning.

A549 tumor-bearing mice were established by subcutaneously injecting 5 × 10<sup>6</sup> of A549 cells into the right flank of each mouse. To analyze ex vivo tumor penetration, the tumors were collected when their average volume had reached 300–400 mm<sup>3</sup>. The excised tumors were cultured for 4 h with IR780-PDMs (DOX-equivalent dose: 5 µg mL<sup>-1</sup>,

IR780-equivalent dose: 2.66 µg mL<sup>-1</sup>) after the medium was adjusted to pH 6.6 or pH 7.4. To analyze in vivo tumor penetration, tumor-bearing mice were administered via intravenous injection with IR780-PDMs at a dose of 1.5 mg DOX kg<sup>-1</sup> and 0.8 mg IR780 kg<sup>-1</sup> for 24 h. Frozen sections of tumors were harvested. The nuclei of the cells were stained with DAPI. The fluorescence of edge and inside region of each tumor section were imaged using Nikon biological microscope.

**In Vivo Imaging and Biodistribution Analysis:** When the tumor volume of A549 tumor-bearing mice reached 100–150 mm<sup>3</sup>, these mice were intravenously injected with IR780+P-DOX and IR780-PDMs at a dose of 0.4 mg IR780 kg<sup>-1</sup>, respectively. The fluorescent images at predetermined time intervals (2, 12, 24, and 36 h) were captured by an in vivo IVIV Lumina II optical imaging system (Caliper, USA). The major organs (heart, liver, spleen, lung, and kidney) and tumors from the above-treated tumor-bearing mice were collected for ex vivo imaging. To capture the in vivo photoacoustic signal at the focal depth of 5 mm at the tumor site after intravenous administration of PBS, IR780+P-DOX, or IR780-PDMs for 24 h, a photoacoustic imaging system (VEVO LAZR-X, Fujifilm VisualSonics, USA) with laser at a wavelength of 720 nm was used.

**Circulation Half-Life and Tumor Retention Study:** Free IR780 was dissolved in cremophor E1 and alcohol mixed solution (50:50, v/v), and then diluted by PBS. The preparation procedure of IR780-Ms was similar to the IR780-PDMs. PDEA-*b*-POEGMA and IR780 were dissolved in acetone, and then slowly injected into deionized water. The stock solution was stirred to evaporate the acetone completely. Female BALB/c mice were intravenously administered with free IR780, IR780-Ms, or IR780-PDMs at a dose of 0.8 mg IR780 kg<sup>-1</sup>, respectively. 10 µL of blood sample from each mouse was collected into heparinized centrifuge tube at each of the following time points: 0.2, 0.5, 1, 2, 4, 8, 12, and 24 h after dosing. All blood samples were stored at 4 °C before analysis. The fluorescence intensity of each sample in the centrifuge tube was measured using a Bruker F PRO imaging system (Billerica, MA, USA). The percent injected dose (%ID) was calculated using the following equation: %ID = (dose in blood) / (injected dose) × 100%.

A549 tumor-bearing mice were intravenously injected with free IR780, IR780-Ms, and IR780-PDMs at a dose of 0.4 mg IR780 kg<sup>-1</sup>, respectively. The fluorescent images at predetermined time intervals were captured by an in vivo IVIV Lumina II optical imaging system to evaluate the tumor retention of the drug formulations.

**Chemo-Photothermal Synergistic Therapy:** When the tumor volumes reached 100–150 mm<sup>3</sup>, A549 tumor-bearing mice were randomly divided into seven groups (*n* = 3), and separately administered via tail vein injection with PBS, DOX, IR780+P-DOX, and IR780-PDMs at a dose of 1.5 mg DOX kg<sup>-1</sup> and 0.8 mg IR780 kg<sup>-1</sup> (designated as the day 0). In the case of PBS, IR780+P-DOX, and IR780-PDMs groups, the tumors were exposed to the NIR laser with 1 W cm<sup>-2</sup> for 5 min at 24 h postinjection. The temperature and IR images were recorded in real time using an infrared camera. Afterward, the tumor size and body weight of each mouse were monitored and recorded every 2 days. The tumor size was measured by a vernier caliper, and the tumor volume (*V*) was estimated using the formula: *V* = (length × width<sup>2</sup>)/2. The isolated solid tumors from the nude mice were weighted at the end of treatment.

**Histological Analysis:** The harvested tumors and major organs of mice were fixed in 5% paraformaldehyde solution and then embedded into paraffin. These tissues were sectioned at a thickness of 5 µm, and separately stained with H&E and TUNEL to assess the histological alteration.

**Statistical Analyses:** Data were given as mean ± standard deviation (*n* ≥ 3). The statistical significance of these data was determined by Student's *T*-test. *p* < 0.05 was considered as significant, and *p* < 0.01 was considered as highly significant (GraphPad Prism, version 7.0).

## Supporting Information

Supporting Information is available from the Wiley Online Library or from the author.

## Acknowledgements

C.S. and Y.L. contributed equally to this work. The authors acknowledge the financial support of the National Key Basic Research Program (no. 2017FYA0205301 and no. 2010CB933901), the Natural Science Foundation of China (no. 81921002 and no. 81327002), and the China Postdoctoral Science Foundation (no. 2018M642026).

## Conflict of Interest

The authors declare no conflict of interest.

## Keywords

long-circulating micelles, pH sensitivity, synergistic therapy, tumor penetration,  $\pi$ - $\pi$  stacking

Received: August 2, 2019

Revised: December 19, 2019

Published online:

- [1] a) D. Peer, J. M. Karp, S. Hong, O. C. Farokhzad, R. Margalit, R. Langer, *Nat. Nanotechnol.* **2007**, *2*, 751; b) M. Zhang, X. Zang, M. Wang, Z. Li, M. Qiao, H. Hu, D. Chen, *J. Mater. Chem. B* **2019**, *7*, 2421.
- [2] a) S. Wilhelm, A. J. Tavares, Q. Dai, S. Ohta, J. Audet, H. F. Dvorak, W. C. W. Chan, *Nat. Rev. Mater.* **2016**, *1*, 16014; b) J. Liu, M. Li, Z. Luo, L. Dai, X. Guo, K. Cai, *Nano Today* **2017**, *15*, 56.
- [3] Y. Zhang, T. Ren, J. Gou, L. Zhang, X. Tao, B. Tian, P. Tian, D. Yu, J. Song, X. Liu, Y. Chao, W. Xiao, X. Tang, *J. Controlled Release* **2017**, *261*, 352.
- [4] Y. Wang, Y. Wu, K. Li, S. Shen, Z. Liu, D. Wu, *Adv. Funct. Mater.* **2019**, *29*, 1805582.
- [5] V. P. Torchilin, *J. Controlled Release* **2001**, *73*, 137.
- [6] a) R. Gref, Y. Minamitake, M. T. Peracchia, V. Trubetskoy, V. Torchilin, R. Langer, *Science* **1994**, *263*, 1600; b) R. Dhandapani, S. Sethuraman, A. Subramanian, *J. Controlled Release* **2019**, *299*, 21; c) J. Hu, Y. Sheng, J. Shi, B. Yu, Z. Yu, G. Liao, *Curr. Drug Metab.* **2018**, *19*, 723.
- [7] Y. Shi, R. van der Meel, B. Theek, E. Oude Blenke, E. H. E. Pieters, M. H. A. M. Fens, J. Ehling, R. M. Schiffelers, G. Storm, C. F. van Nostrum, *ACS Nano* **2015**, *9*, 3740.
- [8] M. B. Schaaf, A. D. Garg, P. Agostinis, *Cell Death Dis.* **2018**, *9*, 115.
- [9] C. Holohan, S. Van Schaeybroeck, D. B. Longley, P. G. Johnston, *Nat. Rev. Cancer* **2013**, *13*, 714.
- [10] a) Y. Liu, P. Bhattacharai, Z. Dai, X. Chen, *Chem. Soc. Rev.* **2019**, *48*, 2053; b) Q. Lei, S. B. Wang, J. J. Hu, Y. X. Lin, C. H. Zhu, L. Rong, X. Z. Zhang, *ACS Nano* **2017**, *11*, 7201.
- [11] X. Song, Q. Chen, Z. Liu, *Nano Res.* **2015**, *8*, 340.
- [12] a) T. Li, J. Zhou, C. Zhang, X. Zhi, J. Niu, H. Fu, J. Song, D. Cui, *NPG Asia Mater.* **2018**, *10*, 1046; b) G. Liu, S. Zhang, Y. Shi, X. Huang, Y. Tang, P. Chen, W. Si, W. Huang, X. Dong, *Adv. Funct. Mater.* **2018**, *28*, 1804317; c) J. Peng, Y. Xiao, W. Li, Q. Yang, L. Tan, Y. Jia, Y. Qu, Z. Qian, *Adv. Sci.* **2018**, *5*, 1700891.
- [13] Z. Gu, S. Zhu, L. Yan, F. Zhao, Y. Zhao, *Adv. Mater.* **2019**, *31*, 1800662.
- [14] L. Schaaf, M. Schwab, C. Ulmer, S. Heine, T. E. Mürdter, J. O. Schmid, G. Sauer, W. E. Aulitzky, H. van der Kuip, *Cancer Res.* **2016**, *76*, 2868.
- [15] W. Fan, B. Yung, P. Huang, X. Chen, *Chem. Rev.* **2017**, *117*, 13566.
- [16] a) Q. Liang, N. Bie, T. Yong, K. Tang, X. Shi, Z. Wei, H. Jia, X. Zhang, H. Zhao, W. Huang, L. Gan, B. Huang, X. Yang, *Nat. Biomed. Eng.* **2019**, *3*, 729; b) R. K. Jain, T. Stylianopoulos, *Nat. Rev. Clin. Oncol.* **2010**, *7*, 653; c) J. Wang, W. Mao, L. L. Lock, J. Tang, M. Sui, W. Sun, H. Cui, D. Xu, Y. Shen, *ACS Nano* **2015**, *9*, 7195.
- [17] L. Y. Zhao, Y. M. Liu, R. Chang, R. R. Xing, X. H. Yan, *Adv. Funct. Mater.* **2019**, *29*, 12.
- [18] a) W. Cliff, S. Triantafyllos, C. Jian, M. John, V. P. Chauhan, J. Wen, P. Zoran, R. K. Jain, M. G. Bawendi, F. Dai, *Proc. Natl. Acad. Sci. U. S. A.* **2011**, *108*, 2426; b) S. Qihang, S. Xuanrong, M. Xinpeng, Z. Zhuxian, J. Erlei, Z. Bo, S. Youqing, E. A. Van Kirk, W. J. Murdoch, J. R. Lott, *Adv. Mater.* **2014**, *26*, 7615.
- [19] G. Chen, Y. Wang, R. Xie, S. Gong, *J. Controlled Release* **2017**, *259*, 105.
- [20] a) J. Xu, W. Zhao, J. Sun, Y. Huang, P. Wang, R. Venkataraman, D. Yang, X. Ma, A. Rana, S. Li, *J. Controlled Release* **2018**, *288*, 212; b) X. Wan, Y. Min, H. Bludau, A. Keith, S. S. Sheiko, R. Jordan, A. Z. Wang, M. Sokolsky-Papkov, A. V. Kabanov, *ACS Nano* **2016**, *12*, 2426; c) Y. T. Tam, J. Gao, G. S. Kwon, *J. Am. Chem. Soc.* **2016**, *138*, 8674; d) W. Li, L. Huang, X. Ying, Y. Jian, Y. Hong, F. Hu, Y. Du, *Angew. Chem., Int. Ed.* **2015**, *54*, 3126.
- [21] C. Song, T. Lin, Q. Zhang, S. Thayumanavan, L. Ren, *J. Controlled Release* **2019**, *293*, 1.
- [22] L. Zhang, S. Li, X. Chen, T. Wang, L. Li, Z. Su, C. Wang, *Adv. Funct. Mater.* **2018**, *28*, 1803815.
- [23] D. Hühn, K. Kantner, C. Geidel, S. Brandholt, I. De Cock, S. J. H. Soenen, P. Rivera\_Gil, J.-M. Montenegro, K. Braeckmans, K. Müllen, *ACS Nano* **2013**, *7*, 3253.
- [24] J. Li, S. Zhang, G. Lykotrafitis, G. Bao, S. Suresh, *Adv. Mater.* **2009**, *21*, 419.
- [25] a) J. Wang, F. Chen, L. Liu, C. Qi, B. Wang, X. Yan, C. Huang, W. Hou, M. Q. Zhang, Y. Chen, Y. Du, *Biomaterials* **2016**, *91*, 11; b) C. W. Wong, H. W. Han, Y. W. Tien, S. H. Hsu, *Biomaterials* **2019**, *213*, 119202; c) B. Delalat, C. Cozzi, S. Rasi Ghaemi, G. Polito, F. H. Kriel, T. D. Michl, F. J. Harding, C. Priest, G. Barillaro, N. H. Voelcker, *Adv. Funct. Mater.* **2018**, *28*, 1801825.
- [26] H. J. Li, J. Z. Du, J. Liu, X. J. Du, S. Shen, Y. H. Zhu, X. Wang, X. Ye, S. Nie, J. Wang, *ACS Nano* **2016**, *10*, 6753.
- [27] M. Maturi, E. Locatelli, I. Monaco, M. Comes Franchini, *Biomater. Sci.* **2019**, *7*, 1746.
- [28] a) D. Depan, J. Shah, R. D. K. Misra, *Mater. Sci. Eng., C* **2011**, *31*, 1305; b) H. Zheng, S. Li, Y. Pu, Y. Lai, B. He, Z. Gu, *Eur. J. Pharm. Biopharm.* **2014**, *87*, 454.
- [29] Z. Zhang, J. Wang, C. Chen, *Adv. Mater.* **2013**, *25*, 3869.
- [30] D. Wang, B. Liu, Y. Ma, C. Wu, Q. Mou, H. Deng, R. Wang, D. Yan, C. Zhang, X. Zhu, *J. Am. Chem. Soc.* **2017**, *139*, 14021.
- [31] a) H. Yang, Q. Wang, Z. Li, F. Li, D. Wu, M. Fan, A. Zheng, B. Huang, L. Gan, Y. Zhao, X. Yang, *Nano Lett.* **2018**, *18*, 7909; b) P. Zhang, J. Li, M. Ghazwani, W. Zhao, Y. Huang, X. Zhang, R. Venkataraman, S. Li, *Biomaterials* **2015**, *67*, 104; c) C. Yue, P. L. M. Zheng, P. Zhao, Y. Wang, Y. Ma, L. Cai, *Biomaterials* **2013**, *34*, 6853.
- [32] N. Kuhl, S. Bode, R. K. Bose, J. Vitz, A. Seifert, S. Hoepfner, S. J. Garcia, S. Spange, S. van der Zwaag, M. D. Hager, U. S. Schubert, *Adv. Funct. Mater.* **2015**, *25*, 3295.